RSC Advances

RSC Publishing

PAPER

View Article Online
View Journal | View Issue

In situ hollow fiber membrane facilitated CO_2 delivery to a cyanobacterium for enhanced productivity

Cite this: *RSC Advances*, 2013, **3**, 13203

Michael Kalontarov,[a] Devin F. R. Doud,[b] Erica E. Jung,[a] Largus T. Angenent[b] and David Erickson*[a]

Received 25th January 2013,
Accepted 29th May 2013

DOI: 10.1039/c3ra40454d

www.rsc.org/advances

Recently, cyanobacteria have been metabolically engineered to secrete valuable biofuel precursors eliminating the requirement to harvest and post-process algal biomass. However, development of new photobioreactors (PBRs) that can efficiently deliver light and address the mass transport challenges associated with maintaining high cyanobacteria productivity has been lagging. Hollow fiber membranes (HFMs) are a method for bubble-less gas exchange which has been shown to be effective at enhancing mass transfer. Previous applications of HFM technology to PBRs have been limited to exploring its ability to enhance CO_2 delivery to the bulk liquid volume. To investigate potential strategies for novel PBR design configurations, we examined the growth pattern of *Synechococcus elongatus* around individual HFMs to determine the optimal spacing and conditions for maximizing photosynthetic activity. We have shown that a single fiber enabling passive transport from/to the atmosphere can provide enough gas exchange to increase biomass accumulation by >2.5 times with respect to a non-fiber control. This increased growth was found to decay in the radial direction with the enhanced growth area spanning between 1.2 mm and 1.7 mm depending on the initial inoculation concentration.

Introduction

Biofuels have been proposed as a solution to problems arising from fossil fuel usage such as CO_2 emissions, climate change, and energy security.[1] These fuels are derived from photoautotrophic organisms that fix inorganic carbon (CO_2) into useful biomolecules, and therefore these biofuels have the potential to be carbon neutral.[2] The most common organisms used for this purpose are plant crops. However, their usage has come under widespread scrutiny for two reasons: i) inefficiencies associated with crop-based biofuel production;[3] and ii) competition for land use with traditional agriculture, thereby putting pressure on the food supply, encouraging deforestation, and increasing carbon emissions.[4] The use of photosynthetic microorganisms, such as cyanobacteria and microalgae address both of these problems with their high CO_2 fixation efficiencies, fast growth rates, and potential to utilize waste-water or industrial gas wastes as nutrient sources.[2] Currently, the most developed method for harnessing the energy producing capabilities of these organisms is to convert their stored lipids into biodiesel.[5]

Two major limitations for the widespread adoption of algal biodiesel are inefficiencies in lipid extraction and biomass cultivation.[6] Technologies that allow for direct extraction of soluble biofuels, or biofuel precursors, from a photobioreactor (PBR) could mitigate the difficulties that arise during the extraction/dewatering/refinement processes inherent to biodiesel production. One such advance comes with the development of engineered strains of cyanobacteria that have the ability to directly secrete fuels such as hydrogen,[7,8] ethanol,[9,10] isobutyraldehyde[11] and other high value products.[12] Specifically, isobutyraldehyde production in an engineered strain of *Synechococcus elongatus* has been performed at area-wise efficiencies comparable to or greater than bioethanol and biodiesel.[13] In parallel with these advances, limitations in biomass cultivation could be addressed by improving the state-of-the-art in bioreactor engineering.

Algal biomass is most commonly cultivated in open raceway ponds and tubular PBRs.[14] Open pond reactors offer a low cost and low energy approach, but also low productivity, while tubular PBRs offer much higher productivity at the cost of high energy and capital input.[15] To improve biomass cultivation, the fundamental limitations that need to be addressed by new PBR designs are efficient delivery of light and inorganic carbon to the bacteria, and the removal of dissolved oxygen and other products including soluble fuels.[16] These limitations can be addressed by creating ultra-compact PBRs that attempt to enhance transport of both light and nutrients, and facilitate the extraction of products at the bacterial scale to increase volumetric and footprint efficiencies. We have recently demonstrated an architecture by which light can be delivered to a bacterial layer in a compact

[a]*Sibley School of Mechanical and Aerospace Engineering, Cornell University, Ithaca, New York, 14853, USA. E-mail: de54@cornell.edu*
[b]*Department of Biological and Environmental Engineering, Cornell University, Ithaca, New York, 14853, USA*

manner.[17] The work presented here attempts to compliment this technology by addressing limitations in inorganic carbon transport.

The typical method for inorganic carbon delivery used in open ponds and tubular PBR designs is the aeration of growth media by exposure to the atmosphere or bubbling.[18] Though this has been shown to be effective, disadvantages include inefficiencies with incomplete CO_2 utilization or losses to the atmosphere (depending on whether an open or closed system approach is used), and unequal transport throughout the reactor.[19] Hollow fiber membranes (HFMs) are a technology that allow for bubble-less gas exchange and have been used in a wide variety of engineering and bio-engineering applications including the treatment of wastewater[20] and landfills.[21] HFMs are attractive for photobioreactor engineering since they allow for both CO_2 delivery and O_2 removal as a function of their partial pressures across the membrane.[22,23] In addition, another potential advantage is the ability to extract soluble products using compatible HFMs. In the last decade, researchers have applied HFM technology to photobioreactors by incorporating HFM modules and have demonstrated improved CO_2 sequestration and biomass growth rate with a range of cyanobacteria and microalgae.[23–26]

Several parameters have to be optimized to directly apply HFMs in compact reactor designs. Chief among them is the maximum spacing that can separate the fibers while still maintaining an adequate gas exchange rate to support photosynthetic growth and fuel production. Having fibers spaced farther apart than optimum would result in zones of low CO_2 concentration and limited productivity. On the other hand, a closer spacing of the fibers would result in an inefficient use of reactor volume since more of the reactor space would be used up by the fibers unnecessarily. In this study, we characterized the growth of *S. elongatus* in CO_2 limited conditions where a single HFM fiber served as the only CO_2 source. Changes in the bacterial distribution as a function of time for several initial bacteria concentrations were characterized and compared to controls.

Materials and methods

The experimental setup consisted of sealed miniature reactors measuring 40 mm × 16 mm × 6 mm. A single HFM fiber (model no. MHF304KM purchased from the Mitsubishi Rayon Co., Ltd.) centered on the bottom of the reactors along the primary axis (Fig. 1), was exposed to the atmosphere on both sides and used for passive gas delivery throughout the course of the experiments. The MHF304KM is a multilayered composite hollow fiber membrane, composed of a non-porous ultra-thin membrane sandwiched between two porous membranes. The reactors were constructed with a microscope glass slide foundation and a PDMS chamber positioned on top. The HFM fiber was aligned in between the center of the PDMS cover and glass slide. A glass cover-slip was fixed atop the PDMS ceiling to reduce gas diffusion into the reactor. All walls and joints were sealed with KwikWeld Epoxy (J–B Weld Company) to make the reactors as gas tight as possible. Reactors without the HFM fiber served as controls for CO_2 delivery. *Synechococcus elongatus* SA665, which has been engineered to produce isobutyraldehyde from CO_2, was obtained from the Liao lab at UCLA.[11] The reactors were inoculated with *S. elongatus* SA665 resuspended in modified BG-11 media with no carbon and the addition of a 50 mM

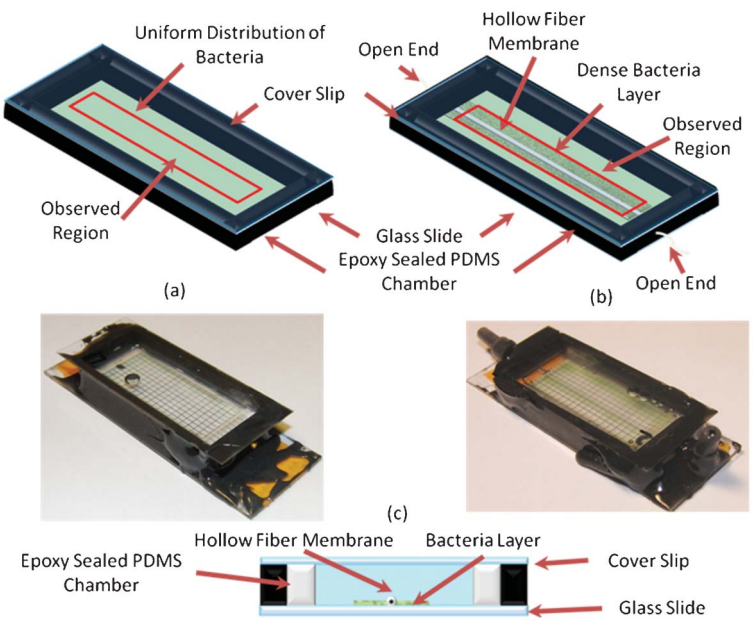

Fig. 1 Experimental and control reactors: Schematic representation of the reactors, with the observed region indicated and photographs after 5 days of growth. (a) Fiber-less control reactors. (b) Reactors with a fiber showing a dense layer forming next to the fiber. (c) *Z*-axis cross-section of the reactor.

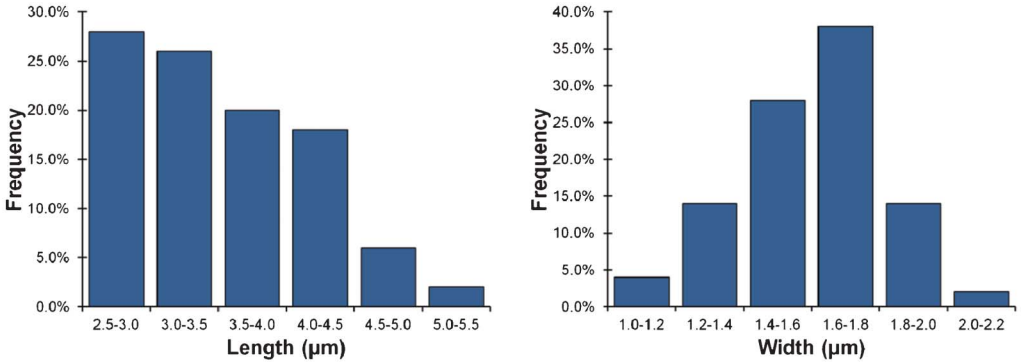

Fig. 2 *S. elongatus* size distribution (n = 50).

phosphate buffer (pH 7.0).[11] The media was made carbon free by eliminating bicarbonate and by sparging with N_2 for 30 min in an anaerobic serum bottle prior to re-suspension and inoculation of *S. elongatus*. Bacteria grown in this media are CO_2 limited and only experience growth at sources of CO_2 flux, only two of which exist in our reactors: the fiber and the reactor walls. As will be illustrated in Fig. 3(b) and Fig. 4(a) the flux through the walls is very limited so the bacteria do not experience a continuous growth phase in the non-fiber reactors.

After inoculation was completed the reactors were sealed, shaken for a uniform initial distribution, and placed into either light or dark conditions. Two fluorescent light strips (American Fluorescent Plug-in Light Strip), which were positioned above the reactors, provided uniform illumination. Photon flux density in the plane of the reactors was measured to be 75 μE s^{-1} m^{-2}. The reactors were operated at laboratory room temperature measured to be 25 °C. Growth in the reactors was imaged *via* chlorophyll fluorescence under an upright fluorescence microscope (Olympus BX51) using a 5x objective and a CCD camera (Sony XCD-X710). Excitation light was provided by a mercury lamp and a Chroma Cy5 filter cube was used to filter the excitation (620 nm, 60 nm bandwidth) and emission (720 nm, 75 nm bandwidth) light. High contrast images of the bacteria in reactor were used to characterize the bacterial distribution along the length of the fiber. The images had a pixel resolution of ~1.8 μm, and this allowed for adequate imaging the bacteria, which have average dimensions of 3.5 ± 1.6 μm in length and 1.7 ± 0.2 μm in width, while also allowing us to observe a large extent of the reactor. Fig. 2 depicts the bacteria size distribution. Bacteria whose size is much smaller than the average would lead to partially covered pixels, and this will introduce some error in our image processing.

Surface density, which represents the percentage of the two-dimensional reactor area that is covered by bacteria, was used to quantify bacterial growth. This quantity was calculated locally by first dividing the obtained fluorescence images into 128-by-128 pixel squares, corresponding to a physical area of approximately 235-by-235 μm. In each square we identified the

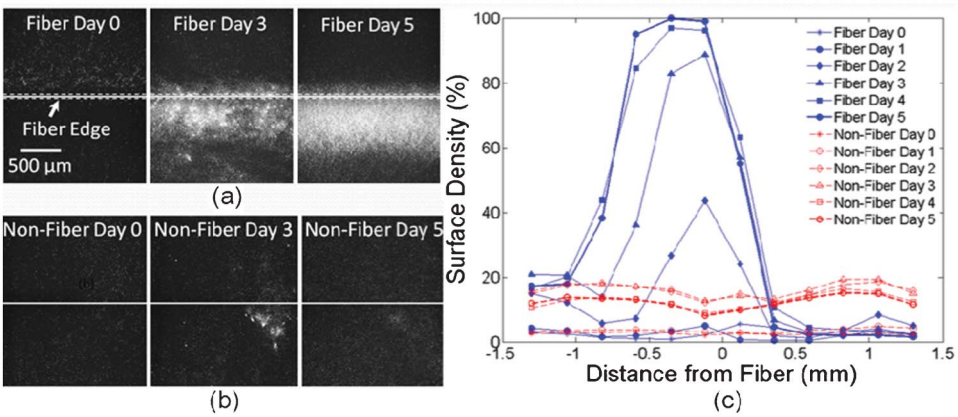

Fig. 3 Cross-section of bacterial distribution perpendicular to fiber direction in light exposed reactors. Bacteria distribution in the middle of two sample reactors (imaged from the top): (a) the bacteria organize into a dense layer close to the fiber in fiber-equipped reactors (note fiber not seen as images are aligned to the fiber's edge), (b) in non-fiber reactors the bacteria take on a random distribution. (c) Quantitative representation of change in the cross-sectional surface density for the two sample reactors with time (distance is from center axis of the chip for the non-fiber reactor). The data points are averages across the total length of the observed region.

pixels containing bacteria and divided by the total number of pixels in the square to obtain the local surface density expressed as a percentage. The fluorescence intensity of each pixel was used only in a binary fashion in our analysis to identify whether bacteria are present. This allowed us to map out the area next to the fiber and develop a grid description of the bacterial distribution. If a pixel is covered by more than one bacteria, that pixel is only counted once in the surface density calculation because surface density is inherently a 2D quantity. The area of interest that was observed was a rectangle of approximately 2.8 mm-by-26 mm that was centered on the fiber and corresponded to a grid of 12 by 112 squares for which the local surface density was calculated. The width of this rectangle had been determined to be the range over which to monitor growth during preliminary experiments. The observed rectangle was offset from all of the walls of the reactor by a minimum of 5 mm. Preliminary experiments were done to confirm that this offset was long enough to prevent edge effects from interfering with the observed region. By averaging the local surface density over the area of interest, we obtained the total surface density.

We conducted trials with a range of reactor inoculation values corresponding to initial surface densities of 0.35%, 2.5%, and 6.0% coverage. This allowed us to characterize effects of CO_2 delivery from the fiber on growth for over an order of magnitude variation in the starting concentration, specifically to see if growth became limited at higher densities. Each trial consisted of 9 reactors placed in the dark, and 9 placed in the light. In each case, 6 reactors had fibers and 3 did not. The reactors placed in the dark served as the controls for carryover growth from the pre-culture and settling out patterns of bacteria as opposed to growth. The reactors without fibers served as controls for determining the baseline amount of growth occurring without the presence of a HFM. All reactors were imaged daily using a microscope for 6 consecutive days.

Results and discussion

Characterization of photosynthetic growth distribution

Photosynthetic growth of *S. elongatus* adjacent to a single HFM delivering CO_2 is reported here (Fig. 3 (a)). Following inoculation, *S. elongatus* randomly settled on the bottom of the reactor. After 2 days, a more concentrated band of growth formed close to the fiber. This layer continued to expand throughout the fifth day of the experiment. While the initial distribution in the fiber and non-fiber reactors began similarly, they diverged on day 2 with the bacteria distributing into a random pattern and ceasing to grow in the fiber-less reactor (Fig. 3 (b)). To observe the increased growth adjacent to the entire length of the fiber, we averaged the local cross-sectional distributions together (Fig. 3 (c)). The trends for the average cross-section distributions are the same as those presented for the local distributions shown in the images of the bacteria. This growth area corresponds to the dimensions over which the HFM can provide effective passive gas exchange for sustained growth. The bacteria in the initial distribution are in a monolayer in both the fiber and non-fiber reactors. In the high surface density layers that develop in the fiber-equipped reactors the bacteria are present in a multilayer. The multilayer is not an intact film, and though a small percentage of cells permanently adhere to the surface the cells can be separated from the surface and each other with sufficient agitation. In the non-fiber reactor the bacteria remain in a low surface density monolayer.

In the light, fiber equipped reactors outgrew non-fiber controls by 3.3, 3.4 and 2.7 times for 6.0%, 2.5% and 0.35% surface densities respectively (p-value < 0.05) (Fig. 4(a)). Increasing the initial *S. elongatus* concentration from 0.35%

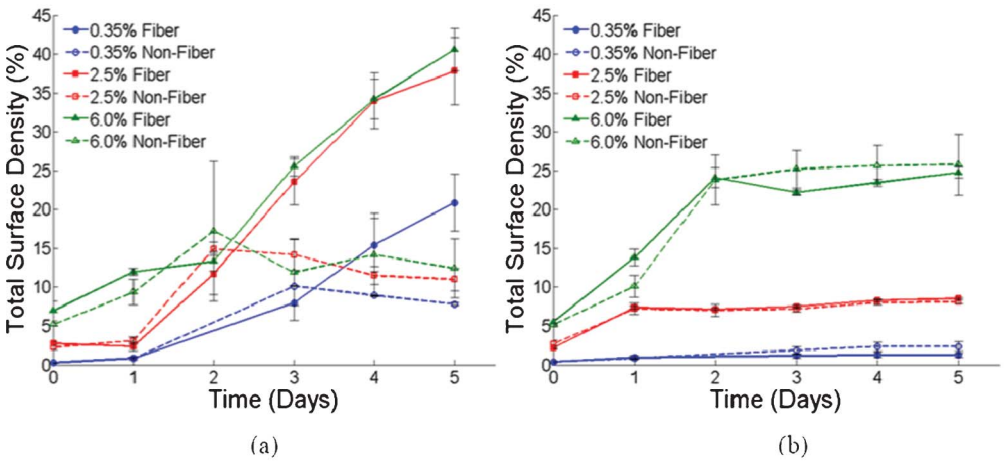

Fig. 4 Total surface density with respect to time: The percent of area covered with bacteria was measured on a daily basis. (a) When exposed to light the reactors equipped with fibers outperformed the non-fiber reactors and grew continuously over the observation period. This trend was illustrated with images of these reactors in Fig. 2. (b) In the dark, the difference between fiber and fiber-less reactors was negligible. For the reactors kept in the dark the increase in bacterial surface density was attributed to gravity driven settling of bacteria and carryover growth. Error bars represent the standard error of the mean.

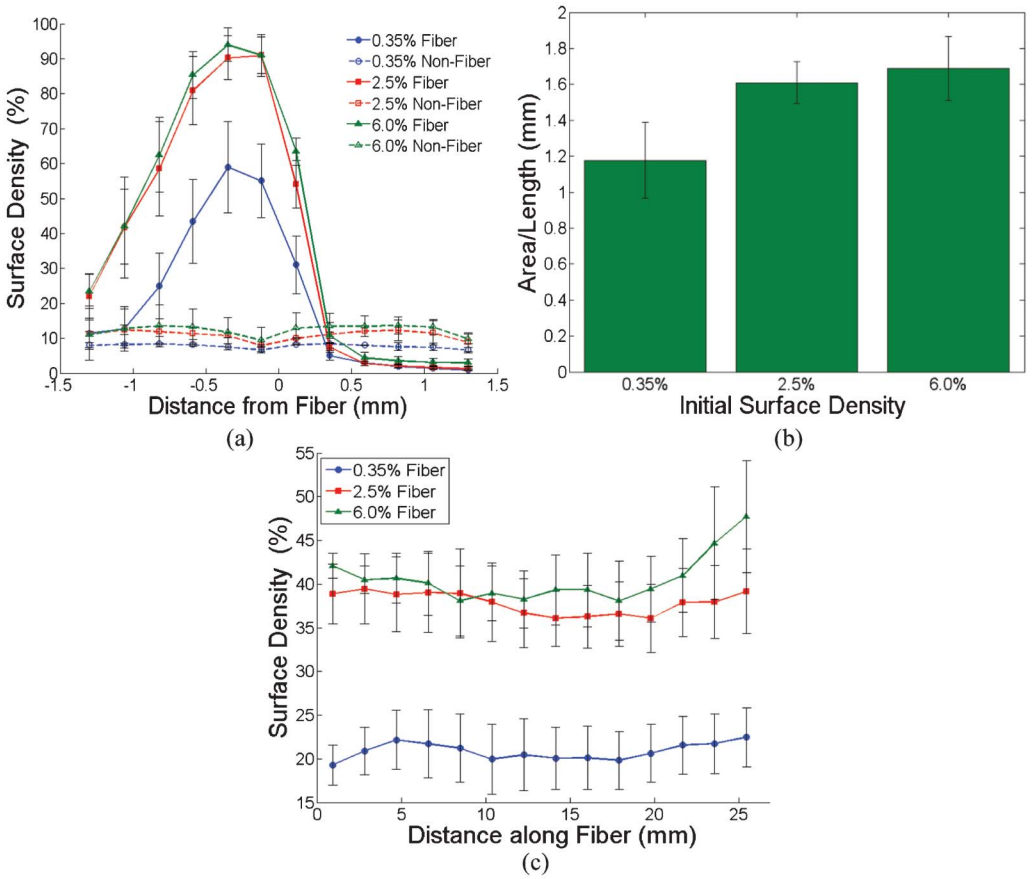

Fig. 5 Final bacterial distribution after 5 elapsed days (observed region is 26 mm by 2.8 mm centered on fiber): (a) The comparison of the final cross-sectional distributions for the fiber and non-fiber reactors indicates that a region of enhanced growth develops on one side of the fiber. (b) The size of enhanced growth region is quantified as an area per length of fiber in which such growth occurs. (c) The lengthwise distribution does not exhibit a strong trend in the fiber reactors and serves to confirm that the cross-sectional distributions shown here persist for the length of the observed region. Error bars represent the standard error of the mean.

to 2.5% lead to a higher final surface density; however, a further increase from 2.5% to 6.0% did not significantly change the final surface density. This suggests that surface density saturation around a single fiber was reached after 5 days with a 2.5% starting inoculation under our experimental conditions. Dark controls (Fig. 4(b)) demonstrate the level of surface coverage in these reactors attributed to bacterial settling and carryover growth from the preculture. At each inoculation concentration, an increase in surface coverage of about 5 fold was observed in the dark. This increase in the dark reactors was independent of presence of a fiber but is significantly lower than the growth in the illuminated fiber reactors.

The final average cross-sectional distributions showed distinct shapes depending on whether a fiber is present (Fig. 5 (a)). In reactors without fibers, the distribution was essentially uniform and slightly higher in the case of the higher inoculations. The reactors with fibers, however, were not uniform in their growth patterns and included regions in which very high surface densities were achieved (close to 100% for the 2.5% and 6.0% surface densities). This is evidence of a dense photosynthetically active layer forming next to the fiber. Surprisingly, the distribution of this layer was consistently observed to not be symmetric with respect to the fiber position, and instead peaks slightly to one side of the fiber. Whether the peak is on the right or left side of the fiber varies reactor to reactor, but invariably a dense bacterial layer developed along one side of the fiber. We have chosen to label the side of the fiber with this layer as the negative side in each reactor so that they can be directly compared. This asymmetry could have resulted from a bias in the initial distribution during the inoculation of the reactors; however, this bias is not clearly deduced from the data. The possibility that this was due the fact the cover-slip and the glass slide (forming the ''roof'' and ''floor'') are misaligned and affect the light distribution was considered. However, the misalignment occurs in all 3-axes and measurement of this imperfection across the reactors shows that the worst case deviation is 1 mm over the 24 mm width of the cover slip, which corresponds to a maximum deviation angle of $\sim 2.5^{\circ}$. Such a small imperfection should not affect the light distribution significantly enough to suppress growth completely on one side of the fiber. Furthermore, in reactors filled with standard BG-11 media, in which a carbon source is present, the bacteria distributions are uniform with respect to the fiber.

Analysis and discussion

The presence of a fiber enhanced photosynthetic growth and facilitated formation of a high surface density bacterial layer adjacent to the fiber (Fig. 4 and Fig. 5 (a)). The region of enhanced growth can be quantified as the increase in surface density in the fiber-equipped reactors compared to the uniform surface density in the non-fiber and dark reactors. The area of enhanced growth per unit fiber length was found to be 1.7 $\pm$ 0.2 mm, 1.6 $\pm$ 0.1 mm, and 1.2 $\pm$ 0.2 mm for the 6.0%, 2.5% and 0.35% inoculations, respectively (Fig. 5 (b)). This corresponds to approximately 6, 5.5, and 4 fiber diameters. Increasing the initial surface density from 2.5% to 6.0% did not significantly change the range of the enhanced growth region indicating this result is close to the maximum that could be obtained from a single fiber. Since the diffusion of CO_2 perpendicular to the fiber depends on the partial pressure of CO_2 inside the fiber, the metrics obtained in this experiment only pertain to fibers supplied with atmospheric partial pressure of CO_2. The values for areas of enhanced growth per unit length fiber obtained here can be used to estimate the spacing between fibers that could be used in such a setup. To further show that the cross-sectional data presented is valid over the entire length of the fiber we investigated, we present the lengthwise bacteria distributions in Fig. 5 (c). The variation in the distribution along this axis is within the experimental variability for the cases of the 0.35% and 2.5% initial surface density inoculation with a slight gradient noticeable for the 6.0% case. Any gradient in the lengthwise bacteria distributions would be indicative of a gradient in the partial pressure of CO_2 along the fiber, because, in CO_2 limited growth conditions the growth rate of the bacteria is proportional to the available CO_2 concentration. We observed variations only in the high initial inoculation case (where any changes variation of growth rate along the fiber would be magnified as compared to a lower initial inoculation), which leads us to posit that a close to uniform partial pressure of CO_2 was maintained throughout the entire length of the fiber. In every case, however, the variation in the lengthwise distribution is much less extreme than the variation in the cross-sectional distribution. This is consistent with the fact that the rate of gas transport through the fiber core should encounter less resistance than the rate of transport across the membrane of the fiber and into the liquid phase. Because the length of fiber used in our experiments was only 2.6 cm, a much larger fiber would be needed to support a full scale PBR. With increasing fiber length, a more pronounced variation in the lengthwise partial pressure of CO_2 in the fibers would be expected if only passive transport is provided. However, this limitation could be overcome by active transport of carbon rich gas through the fiber.

In our work, we focused on characterizing growth in the micro-environment adjacent to a single HFM delivering CO_2 in an otherwise carbon starved environment. To compare the observed growth in our miniature reactors to growth in a traditional lab-scale growth chamber, specific growth rates were used as a metric. The specific growth rates in our experiments were calculated by fitting the surface density adjacent to the HFM *versus* time for each trial. Data for days 1–4 was used for this fit, as this was the observed exponential growth phase (Fig. 3(a)). Different specific growth rates were observed to occur with different inoculation concentrations used. The results of these calculations are presented in Table 1 and are compared to the growth rate of *S. elongatus* observed in bubble-aerated, continuously rapidly mixed, culture flasks maintained at a temperature of 35 °C and a similar light flux (50 $\mu E\ s^{-1}\ m^{-2}$) as used in our experiments.[27] Though our miniature reactors operated in CO_2 limited conditions with no active transport methods, the growth rate observed in reactors started at a 0.35% initial surface density was 72% of the observed rate in a traditional laboratory scale reactor.

Recent HFM studies have concentrated on incorporating HFM modules into PBR systems to enhance biomass production by improving CO_2 exchange, regulating pH, and promoting CO_2 fixation. However, the application of the HFMs has thus far only been investigated for their CO_2 delivery to bulk reactor volumes in recirculated PBRs. Table 1 shows specific growth rates from our experiments compared to results previously reported for PBRs utilizing integrated HFM modules, note that since the reactors operate under varying conditions and utilize different strains these numbers should not be used for an absolute comparison. Placed alongside values reported from previous HFM experiments the calculated growth rates from our experiments were of a similar magnitude. This analysis implies that, although demonstrated on only a small scale, the growth rates achieved in the micro-environment surrounding the fiber are comparable with other HFM reactors and with traditional bubble-aerated laboratory

Table 1 Comparison of Specific Growth Rates

Reactor type	Specific Growth Rate μ (h^{-1})	Reactor volume (mL)
***S. elongatus* Reactors**		
Lab-scale *S. elongatus* growth chamber	~0.0577	120
Our system – initial surface density 0.35%	0.0415 $\pm$ 0.0097	4
Our system – initial surface density 2.5%	0.0376 $\pm$ 0.0045	4
Our system – initial surface density 6.0%	0.0158 $\pm$ 0.0025	4
Recent HFM Reactors		
Membrane-sparged helical tubular photobioreactor (MSTR)[24]	0.0190[a]	800
Hollow fiber membrane photo-bioreactor (HFMPB)[26]	0.0085[b]	500
Membrane carbonation photobioreactor (MCPBR)[25]	0.0083	5500

[a] Estimated from plot. [b] Calculated from reported biomass productivity rate.

setups. It is also important to note that our system operated with no circulation. Adding circulation, as in previous systems, increases mass transfer but impact cost considerations for a scaled up system. Light delivery challenges in a scaled up version could be overcome by using the slab-waveguide system we have previously developed.[17]

Conclusion

In this work, we characterized the ability of a single HFM fiber to enhance the growth of *S. elongatus* in a simple batch reactor with no media circulation. The diffusive transport of atmospheric gas through a single HFM fiber and into the bacteria resulted in the development and sustained growth of a dense bacterial layer along the length of the fiber. We observed this effect over the length of a short fiber distance, but this same effect could potentially be produced by longer fibers after switching to an active rather than passive system of gas transport. This implies that the system should be readily scalable and this conjecture can be tested in future experiments. In conjunction with waveguide provided light, this system could serve as the backbone to a scalable PBR, harboring direct fuel-producing photosynthetic bacteria, operating at high volumetric productivities.

Acknowledgements

This work was supported by the academic venture fund of the David R. Atkinson Center for Sustainable Future and a CAREER grant from the National Science Foundation (NSF) for Optofluidics – Fusing Microfluidics and Photonics (#0846489). The authors would also like to thank the James Liao group at UCLA for providing the *S. elongatus* strain used in this study. We also thank Matthew Mancuso for helpful discussions regarding the experiment and data analysis.

References

1 C. Sheridan, *Nat. Biotechnol.*, 2009, **27**, 1074–1076.
2 L. Brennan and P. Owende, *Renewable Sustainable Energy Rev.*, 2010, **14**, 557–577.
3 T. Searchinger, R. Heimlich, R. A. Houghton, F. Dong, A. Elobeid, J. Fabiosa, S. Tokgoz, D. Hayes and T.-H. Yu, *Science*, 2008, **319**, 1238–1240.
4 J. Fargione, J. Hill, D. Tilman, S. Polasky and P. Hawthorne, *Science*, 2008, **319**, 1235–1238.
5 Y. Chisti, *Biotechnol. Adv.*, 2007, **25**, 294–306.
6 Y. C. Sharma, B. Singh and J. Korstad, *Green Chem.*, 2011, **13**, 2993–3006.
7 M. L. Ghirardi, M. C. Posewitz, P.-C. Maness, A. Dubini, J. Yu and M. Seibert, in *Annual Review of Plant Biology*, 2007, vol. 58, pp. 71–91.
8 K. McNeely, Y. Xu, N. Bennette, D. A. Bryant and G. C. Dismukes, *Appl. Environ. Microbiol.*, 2010, **76**, 5032–5038.
9 M. D. Deng and J. R. Coleman, *Applied and Environmental Microbiology*, 1999, **65**, 523–528.
10 D. X. Luo, Z. S. Hu, D. G. Choi, V. M. Thomas, M. J. Realff and R. R. Chance, *Environ. Sci. Technol.*, 2010, **44**, 8670–8677.
11 S. Atsumi, W. Higashide and J. C. Liao, *Nat. Biotechnol.*, 2009, **27**, 1177–U1142.
12 D. C. Ducat, J. C. Way and P. A. Silver, *Trends Biotechnol.*, 2011, **29**, 95–103.
13 J. Sheehan, *Nat. Biotechnol.*, 2009, **27**, 1128–1129.
14 D. Aitken and B. Antizar-Ladislao, *Energies*, 2012, **5**, 1613–1647.
15 O. Jorquera, A. Kiperstok, E. A. Sales, M. Embirucu and M. L. Ghirardi, *Bioresour. Technol.*, 2010, **101**, 1406–1413.
16 L. Xu, P. J. Weathers, X. R. Xiong and C. Z. Liu, *Eng. Life Sci.*, 2009, **9**, 178–189.
17 E. E. Jung, M. Kalontarov, D. F. R. Doud, M. D. Ooms, L. T. Angenent, D. Sinton and D. Erickson, *Lab Chip*, 2012, **12**, 3740–3745.
18 A. Kumar, S. Ergas, X. Yuan, A. Sahu, Q. O. Zhang, J. Dewulf, F. X. Malcata and H. van Langenhove, *Trends Biotechnol.*, 2010, **28**, 371–380.
19 A. P. Carvalho and F. X. Malcata, *Biotechnol. Prog.*, 2001, **17**, 265–272.
20 H. J. Lin, W. J. Gao, F. G. Meng, B. Q. Liao, K. T. Leung, L. H. Zhao, J. R. Chen and H. C. Hong, *Crit. Rev. Environ. Sci. Technol.*, 2012, **42**, 677–740.
21 F. N. Ahmed and C. Q. Lan, *Desalination*, 2012, **287**, 41–54.
22 A. Gabelman and S. T. Hwang, *J. Membr. Sci.*, 1999, **159**, 61–106.
23 L. H. Fan, Y. T. Zhang, L. H. Cheng, L. Zhang, D. S. Tang and H. L. Chen, *Chem. Eng. Technol.*, 2007, **30**, 1094–1099.
24 L.-H. Fan, Y.-T. Zhang, L. Zhang and H.-L. Chen, *J. Membr. Sci.*, 2008, **325**, 336–345.
25 H. W. Kim, A. K. Marcus, J. H. Shin and B. E. Rittmann, *Environ. Sci. Technol.*, 2011, **45**, 5032–5038.
26 A. Kumar, X. Yuan, A. K. Sahu, S. J. Ergas, J. Dewulf and H. Van Langenhove, *J. Chem. Technol. Biotechnol.*, 2010, **85**, 387–394.
27 T. D. B. MacKenzie, R. A. Burns and D. A. Campbell, *Plant Physiol.*, 2004, **136**, 3301–3312.